Synthesis of Very Small Molybdenum Disulfide Nanoflowers for Hydrogen Evolution Reaction

Tuan Van Nguyen[a], Thang Phan Nguyen[b], Quyet Van Le[c], Dung Van Dao[c], Sang Hyun Ahn[a,], and Soo Young Kim[c,]**

[a]School of Chemical Engineering and Materials Science, Chung-Ang University, 84 Heukseok-ro, Dongjak-gu, Seoul 06974, Republic of Korea

[b]Department of Chemical and Biological Engineering, Gachon University, Seongnam-si, Gyeonggi-do 13120, Republic of Korea

[c]Department of Materials Science and Engineering, Institute of Green Manufacturing Technology, Korea University, 145 Anam-ro, Seongbuk-gu, Seoul 02841, Republic of Korea

*Corresponding Authors

E-mail addresses:

- Sang Hyun Ahn: shahn@cau.ac.kr (SHA)
- Soo Young Kim: sooyoungkim@korea.ac.kr (SYK)

Abbreviations. AMT: ammonium molybdate tetrahydrate; BET: Brunauer−Emmett−Teller; CA: chronoamperometry; CV: cyclic voltammetry; DI: deionized water; EDX: energy-dispersive X-ray spectroscopy; FE–SEM: field emission scanning electron microscopy; HER: hydrogen evolution reaction; LSV: linear sweep voltammetry; NF: nanoflower; SNF: small nanoflower;

Abstract

Among various transition metal dichalcogenides, molybdenum disulfides such as molybdenum disulfide nanoflowers (MoS_2 NFs) can effectively catalyze a hydrogen evolution reaction (HER) because of the abundance, ease of processing, and high catalytic activity of MoS_2. The main disadvantage of using MoS_2 NFs for HER on the industrial scale is their low density and number of active sites. Herein, we propose for the first time a facile, inexpensive, and scalable route for fabricating extremely small MoS_2 NFs (SNFs). The size of the synthesized MoS_2 SNFs (50–70 nm) is much lower than that of conventional MoS_2 NFs (600–950 nm), which significantly increases the number of catalytically active sites. In addition, the in situ doping of N atoms considerably enhances the catalytic activity of the prepared MoS_2 SNFs. MoS_2 SNFs exhibit superior electrocatalytic activity toward HER with a low Tafel slope 49 $mV \cdot dec^{-1}$, an overpotential of 270 mV at a current density of 50 $mA \cdot cm^{-2}$, a large surface area of 98 $m^2 \cdot g^{-1}$, and very high stability in an acidic environment. The obtained results indicate that MoS_2 SNFs can be potentially used for energy storage and electrochemical applications.

Keywords: transition metal dichalcogenide, MoS_2 small nanoflower, large surface area.

TAA: thioacetamide; TEM: transmission electron microscopy; TMD: transition metal dichalcogenide; XPS: X-ray photoelectron spectroscopy; XRD: X-ray diffraction.

1. Introduction

New technologies based on hydrogen energy have recently emerged as viable solutions to the energy crisis. Hydrogen represents one of the key materials for hybrid cars and power and heating applications because of its high energy efficiency, abundance, scalable yield, and environmental friendliness [1-3]. Nowadays, hydrogen gas is mainly obtained by water electrolysis, during which two electrons on the cathode surface interact with protons in solution to generate hydrogen molecules. The working electrode is typically fabricated from noble metals such as those of the platinum group because the electrochemical reaction requires very low voltage to produce hydrogen while saving some energy [4-7]. However, the scarcity, low stability, and high cost of the platinum group metals limit their practical applications in the HER process. Therefore, a prospective catalyst for hydrogen energy technology should exhibit high stability, low cost, ease of processability, and high catalytic activity [8-10]. During last decades, two-dimensional transition metal dichalcogenides (TMDs) have been actively investigated in terms of their applicability in HER because of their low cost, high catalytic activity, and high electrochemical stability under acidic conditions. Among many promising TMD candidates, molybdenum disulfides (MoS_2) with various structures exhibit high performance in HER-related applications [11-15].

Different types of MoS_2 have been investigated by various techniques due to their special catalytic properties caused by the unique electronic structure [16-18]. Exfoliation, chemical vapor deposition, and a hydrothermal method are the most widely used routes to produce MoS_2 materials for water splitting. The main drawbacks of the exfoliation method include a relatively

low yield and difficulty to control the quality of the final product. The chemical vapor deposition method is not safe and requires high fabrication temperatures and expensive equipment. In contrast, the hydrothermal method is characterized by high scalability, low cost, and good controllability [19-21]. Therefore, it has been widely utilized to prepare numerous catalyst materials for water splitting and other chemical applications. Among various MoS_2 structures produced by the hydrothermal method, flower-like MoS_2 nanostructures or MoS_2 nanoflowers (NFs) are most commonly applied for HER studies. MoS_2 NFs possess a unique structure with petals on the surface and excellent catalytic characteristics, which make them suitable for electrochemical applications such as HER, batteries, and supercapacitors [22-26]. However, some properties of MoS_2 including low conductivity and small number of active sites require further improvement.

In this work, we propose a new synthesis process for a unique MoS_2 structure, which contains extremely small nanoflowers (SNFs). The much smaller size of the synthesized MoS_2 SNFs as compared with that of conventional MoS_2 NFs is the key parameter enhancing their electrocatalytic properties because it is directly related to the density of catalytically active sites [27-30]. In addition, the in situ doping of MoS_2 SNFs with nitrogen atoms increased their conductivity and electrocatalytic activity [31, 32]. Conventional MoS_2 NFs were also prepared by the same process with slight modification to compare the catalytic mechanism, structures, and HER performances of both catalysts. The obtained results indicate that the electrocatalytic properties of the fabricated MoS_2 SNFs are superior to those of conventional MoS_2 NFs. Therefore, MoS_2 SNFs can be considered a promising catalytic material for energy storage and electrochemical applications.

2. EXPERIMENTAL SECTION

2.1. Chemicals

Ammonium molybdate tetrahydrate (AMT, $(NH_4)_6Mo_7O_{24}\cdot 4H_2O$), thioacetamide (TAA, CH_3CSNH_2), HCl (37% aqueous solution), NH_3 (28% aqueous solution), ethanol (C_2H_5OH), and Nafion (5% aqueous solution) were purchased from Sigma–Aldrich. Deionized (DI) water was obtained from Millipore Mili-Q. All chemicals were used without further purification.

2.2. Synthesis of MoS_2 SNFs

MoS_2 SNFs were synthesized via a facile one-step hydrothermal method. Appropriate amounts of AMT and TAA were added to a glass beaker containing 15 mL of DI water and stirred for 15 min. After that, HCl (37%) was added to the prepared mixture and continuously stirred for 15 min before transferring into a Teflon autoclave. The autoclave was heated to 270 °C for 24 h inside a furnace and then cooled down to room temperature. The synthesized catalyst was centrifuged at a speed of approximately 8000 RPM in DI water and ethanol three times to eliminate all excessive components. After that, the catalyst was dried at 80 °C and then annealed in inert gas to obtain MoS_2 SNFs. The produced catalyst was stored in a glass vial until further studies. Conventional MoS_2 NFs were also synthesized via the same route but slightly modified by heating to 180 °C and replacing the 37% HCl solution with a 28% NH_3 solution. The exact amounts of all materials used during syntheses are listed in **Table 1**.

Table 1. Materials and reaction temperatures for synthesis of MoS_2 NFs and SNFs.

No	AMT (g)	TAA (g)	H_2O (mL)	NH_3 (mL)	HCl (mL)	t (°C)	Catalyst

1	1	2.5	15	0	3	270	MoS_2 SNFs
2	1	2.5	15	3	0	180	MoS_2 NFs

2.3. Electrochemical measurements

All electrochemical measurements were performed at room temperature using a standard three-electrode electrolytic system and Ivium potentiostat V55630. A saturated calomel electrode, graphite electrode, and the synthesized catalysts on glassy carbon electrodes were employed as the reference, counter, and working electrodes, respectively. The HER activities of MoS_2 SNFs and NFs were evaluated via linear sweep voltammetry (LSV) at scan rate of 10 $mV \cdot s^{-1}$. All measurements were conducted in a 0.5 M H_2SO_4 solution with an iR correction. The stability of MoS_2 SNFs was examined by continuous cyclic voltammetry (CV) at a scan rate of 50 $mV \cdot s^{-1}$ for over 1000 cycles. Thereafter, the stability of the prepared MoS_2 SNFs was continuously evaluated via chronoamperometry (CA) for 12 h. Double-layer capacitance (C_{dl}) values of the studied samples were calculated from the results of CV tests, which were performed in the potential range from 0 to 0.2 V at different scan rates (5, 10, 20, 30, 40, and 50 $mV \cdot s^{-1}$). Additionally, electrochemical impedance spectroscopy (EIS) was conducted in a frequency range of 100 kHz – 0.1 Hz.

2.4. Characterization of MoS_2 NFs and SNFs

X-ray diffraction (XRD) was employed to examine the structures and crystallinities of the prepared MoS_2 SNFs and NFs using a powder X-ray diffractometer with Cu Kα radiation (λ =

0.154 nm). The structures and chemical bonding of the fabricated catalysts were investigated by Raman spectroscopy. X-ray photoelectron spectroscopy (XPS) was conducted to determine the surface compositions of the prepared MoS_2 SNF materials. Field emission scanning electron microscopy (FE–SEM) was employed to comprehensively observe the morphology, size, and shape of the synthesized MoS_2 SNFs at different magnifications and an acceleration voltage of 10 kV. Transmission electron microscopy (TEM) was utilized to determine the structure and elemental distributions on the material surfaces. Specific surface areas of the catalysts were calculated by the Brunauer−Emmett−Teller (BET) method from the adsorption of nitrogen gas on the material's surface obtained in a relative pressure range of 0.02–0.30.

3. Results and Discussion

3.1 Formation mechanism of synthesis process

The formation mechanisms of MoS_2 SNFs and NFs are illustrated in **Figure 1** as below.

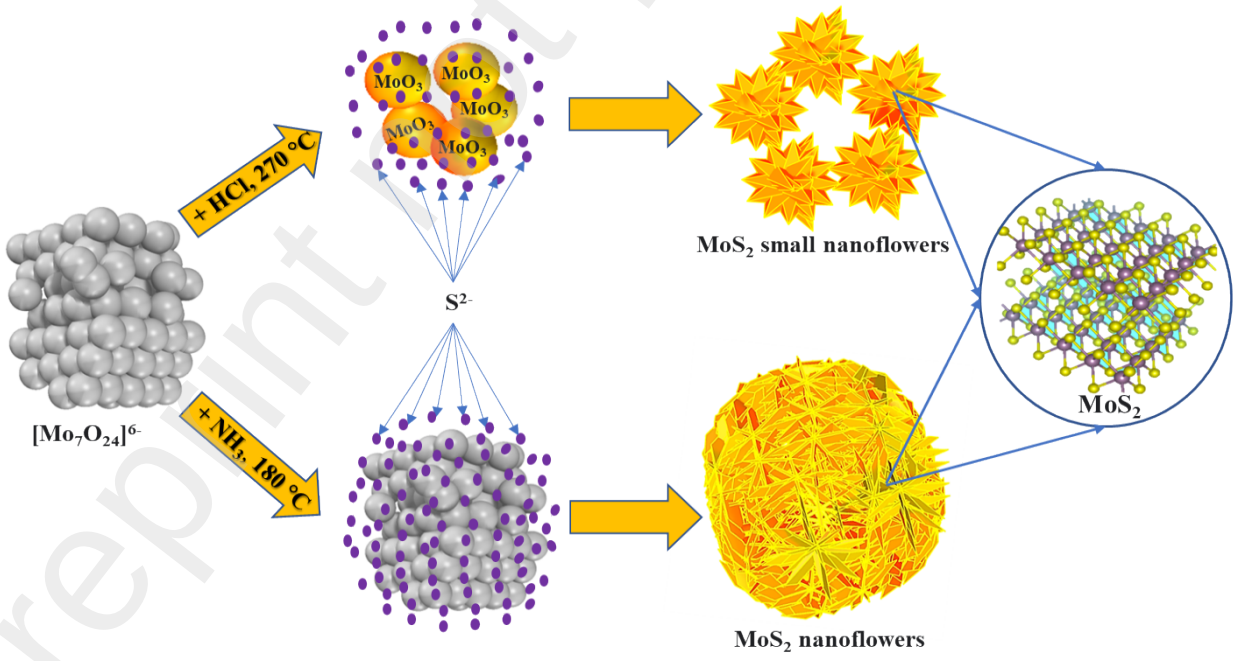

Figure 1: Syntheses and formation mechanisms of MoS_2 SNFs and NFs

It shows that when AMT and TAA were mixed and stirred by a magnetic bar in the neutral solution, both materials decomposed leading to the formation of $[Mo_7O_{24}]^{6-}$, S^{2-}, and H^+ ions due to hydrolysis, as described by Equations (1)–(3) and (1')–(3'). The difference between the two processes was mainly caused by the different temperatures and reagents added in the second step. During the synthesis of MoS_2 SNFs, HCl was added to increase the H^+ concentration, while increasing the temperature to 270 °C induced the reaction described by Equation (5). Consequently, the big anion $[Mo_7O_{24}]^{6-}$ quickly decomposed into a smaller anion and easily reacted with H^+ to form MoO_3 molecules. Next, MoO_3 reacted with S^{2-} to form a MoS_3 intermediate byproduct (6). Finally, MoS_3 was reduced to the final MoS_2 SNF product according to Equation (7). In contrast, for the synthesis of MoS_2 NFs, the NH_3 solution was added to the reaction mixture to increase the NH_4^+ concentration. As a result, the anion $[Mo_7O_{24}]^{6-}$ directly reacted with S^{2-} in the alkaline media to form a large intermediate byproduct MoS_3 as described by Equation (5'), and big MoS_2 NFs were produced via Equation (6'). The formation mechanisms of MoS_2 SNFs and NFs in the autoclave at high temperatures can be briefly summarized by the following equations.

- MoS_2 SNF synthesis process:

$$(NH_4)_6Mo_7O_{24}\cdot 4H_2O \rightarrow 6NH_4^+ + [Mo_7O_{24}]^{6-} + 4H_2O \quad (1)$$

$$CH_3CSNH_2 + 2H_2O \rightarrow H_2S + NH_4^+ + CH_3COO^- \quad (2)$$

$$H_2S \rightarrow S^{2-} + 2H^+ \quad (3)$$

$$HCl \rightarrow H^+ + Cl^- \quad (4)$$

$$[Mo_7O_{24}]^{6-} + 6H^+ \rightarrow 7MoO_3 + 3H_2O \quad (5)$$

$$MoO_3 + 3S^{2-} + 6H^+ \rightarrow MoS_3 \text{ (intermediate)} + 3H_2O \quad (6)$$

$$MoS_3 \rightarrow MoS_2 + S^{2-} \quad (7)$$

❖ MoS_2 NF synthesis process:

$$(NH_4)_6Mo_7O_{24}\cdot 4H_2O \rightarrow 6NH_4^+ + [Mo_7O_{24}]^{6-} + 4H_2O \quad (1')$$

$$CH_3CSNH_2 + 2H_2O \rightarrow H_2S + NH_4^+ + CH_3COO^- \quad (2')$$

$$H_2S \rightarrow S^{2-} + 2H^+ \quad (3')$$

$$NH_3 + H_2O \rightarrow NH_4^+ + OH^- \quad (4')$$

$$[Mo_7O_{24}]^{6-} + 21S^{2-} + 48NH_4^+ \rightarrow 7MoS_3 \text{ (intermediate)} + 48NH_3 + 24H_2O \quad (5')$$

$$MoS_3 \rightarrow MoS_2 + S^{2-} \quad (6')$$

3.2 Phase quantification, chemical composition, and morphology

The crystallinity and phase compositions of the prepared materials were investigated by XRD. As shown in **Figure 2**, the XRD patterns of MoS_2 SNFs and NFs are very similar and contain the peaks centered at 13°, 33°, 40°, 49°, and 58°, which can be assigned to the (002), (100), (103), (105), and (110) planes, respectively. These results indicate that both compounds possess the hexagonal structure of 2H–MoS_2 [JCPDS card no: 01-073-1508], which is in good

agreement with the data obtained in a previous work [33]. The absence of impurity peaks suggests that the synthesized catalysts are very pure. Note that the peaks in the MoS_2 SNFs XRD pattern are sharper than those in the MoS_2 NFs pattern, indicating a higher degree of crystallinity of MoS_2 SNFs [34].

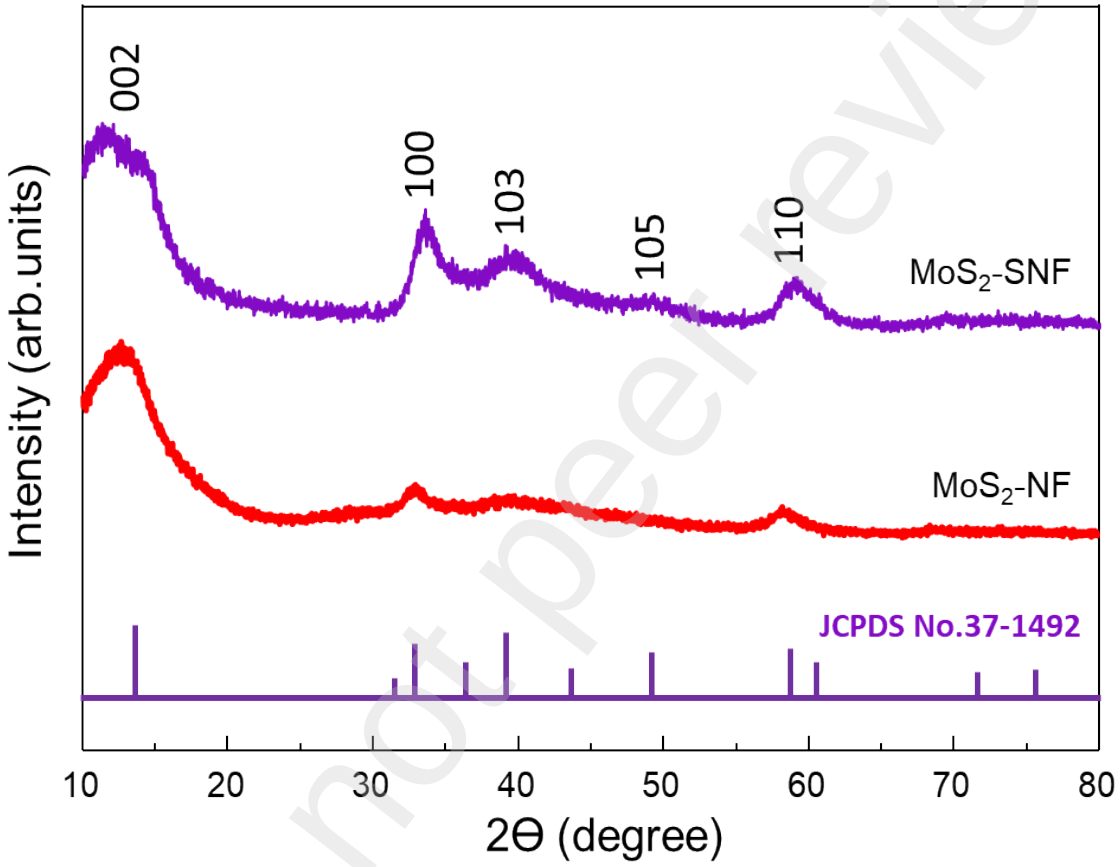

Figure 2. XRD patterns of MoS_2 SNFs and NFs

Raman spectroscopy was performed to further investigate the structures and chemical bonding of the synthesized materials. **Figure 2** shows the Raman spectra of MoS_2 SNFs and NFs. Both compounds exhibit three typical MoS_2 Raman shifts at 284, 336, 377, 402, and 453 cm^{-1}, which correspond to the E_{1g} and A_1 vibrational modes of S atoms with respect to Mo atoms, in-

plane Mo–S vibrational mode (E^1_{2g}), out-of-plane mode A_{2g}, and second-order Raman scattering 2LA(M) mode, respectively [35, 36]. In addition, the Raman peaks located at 198, 236, 284, and 336 cm^{-1} are assigned to the MoO_3 phase, which likely resulted from the surface oxidation of the studied materials or laser-irradiation oxidation during measurements [37].

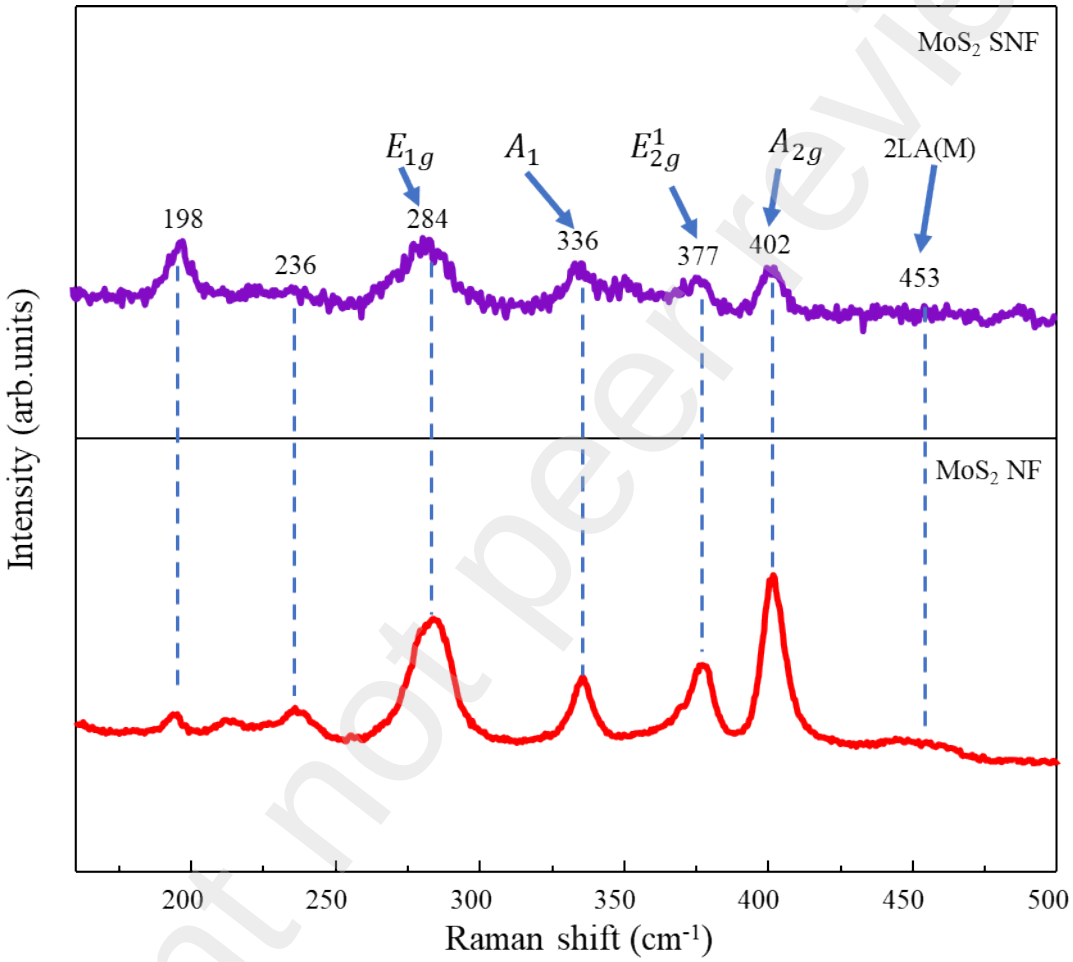

Figure 3. Raman spectra of MoS_2 SNFs and NFs

High-resolution XPS was conducted to determine the composition and atomic valence states of the prepared MoS_2 SNFs. **Figure 4** shows the high-resolution XPS profiles of all elements in the synthesized catalyst. **Figure 4(a)** displays only one pair of Mo 3d peaks located

at 228.9 and 232.2 eV, which can be assigned to the Mo $3d_{5/2}$ and Mo $3d_{3/2}$ states of 2H phase MoS_2, respectively [38, 39]. The absence of Mo^{6+} peaks indicates that all Mo^{6+} species were converted to Mo^{4+} ions during synthesis. The S 2p peak can be fitted to three main peaks centered at 161.8, 163.1, and 164.4 eV corresponding to S $2p_{3/2}$, S $2p_{1/2}$, and edge sulfur, respectively [40]. The presence of nitrogen atoms is confirmed in **Figure 4(c)**. The N 1s peak can be fitted to one peak located around 402.3 eV, which is assigned to oxide nitrogen groups [41]. The O 1s XPS profile can be fitted with two main peaks located at 532.2 and 533.7 eV corresponding to Mo–O and O–H bonds, respectively, which were likely caused by the oxidation of the material surface by the air oxygen [1].

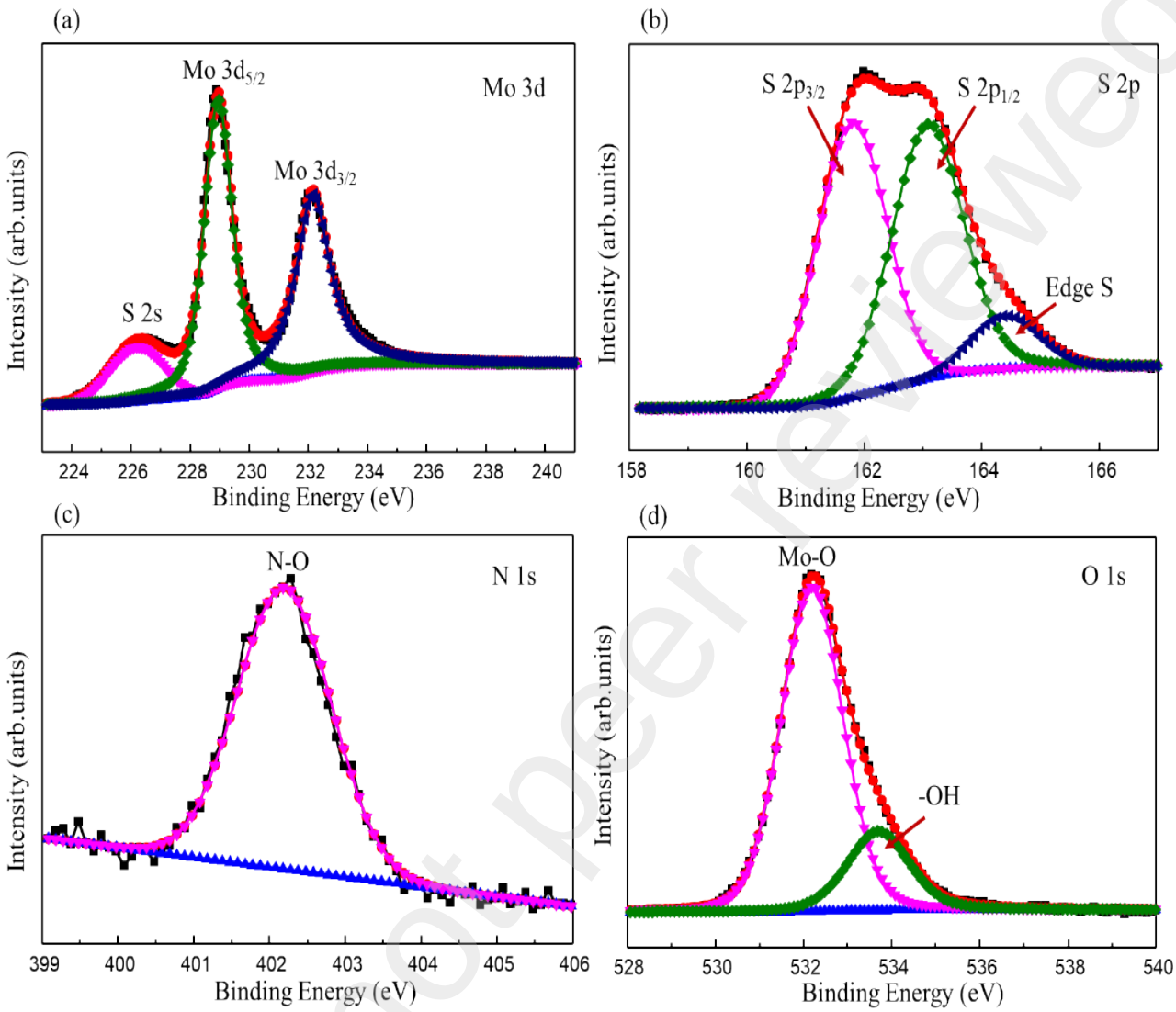

Figure 4. Fitted (a) Mo 3d, (b) S 2p, (c) N 1s, and (d) O 1s XPS peaks of MoS_2 SNFs

The shapes and sizes of the prepared MoS_2 SNFs and NFs were examined by FE–SEM. **Figure 5** shows the FE–SEM images of MoS_2 SNFs obtained at various magnifications and MoS_2 NFs with a scale bar length of 300 nm. MoS_2 NFs exhibit a round surface with numerous petals, which contribute to their electrocatalytic properties. The diameters of MoS_2 NFs vary from 600 to 950 nm. Meanwhile, MoS_2 SNFs also possess a round surface with numerous petals; however, their size does not exceed of 50–70 nm. The extremely small size of MoS_2 increased

the number of catalytically active sites in the electrochemical process, which will be discussed in the next section.

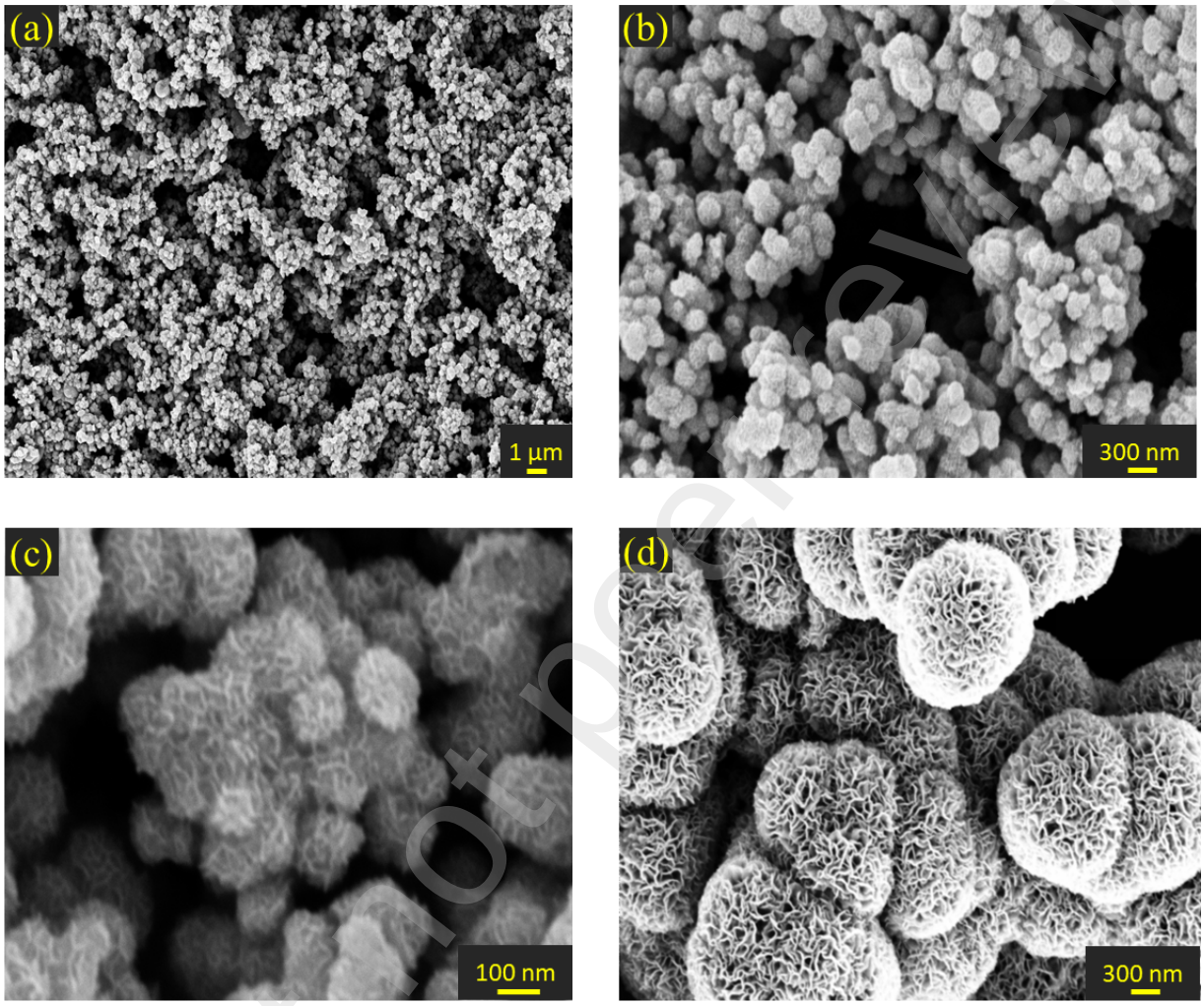

Figure 5. FE–SEM images of (a)–(c) MoS_2 SNFs at different magnifications and (d) MoS_2 NFs

TEM observations were also conducted to investigate the microstructure and crystallinity of the prepared catalysts. **Figures 6(a)–(c)** show the TEM images of MoS_2 SNFs obtained at different magnifications, while **Figure 6(d)** depicts the TEM image of MoS_2 NFs. These results indicate that the size of MoS_2 SNFs is significantly smaller than that of MoS_2 NFs. The high-resolution TEM image (Figure 6a) reveals that the d-spacing of MoS_2 is approximately 0.278 nm,

which can be indexed to the MoS_2 (100) plane. The energy-dispersive X-ray spectroscopy (EDX) pattern displayed in **Figure 6(e)** also confirms the successful synthesis of pure MoS_2 SNFs. **Figures 6(f)–(h)** show the uniform distributions of Mo and S elements on the catalyst surface.

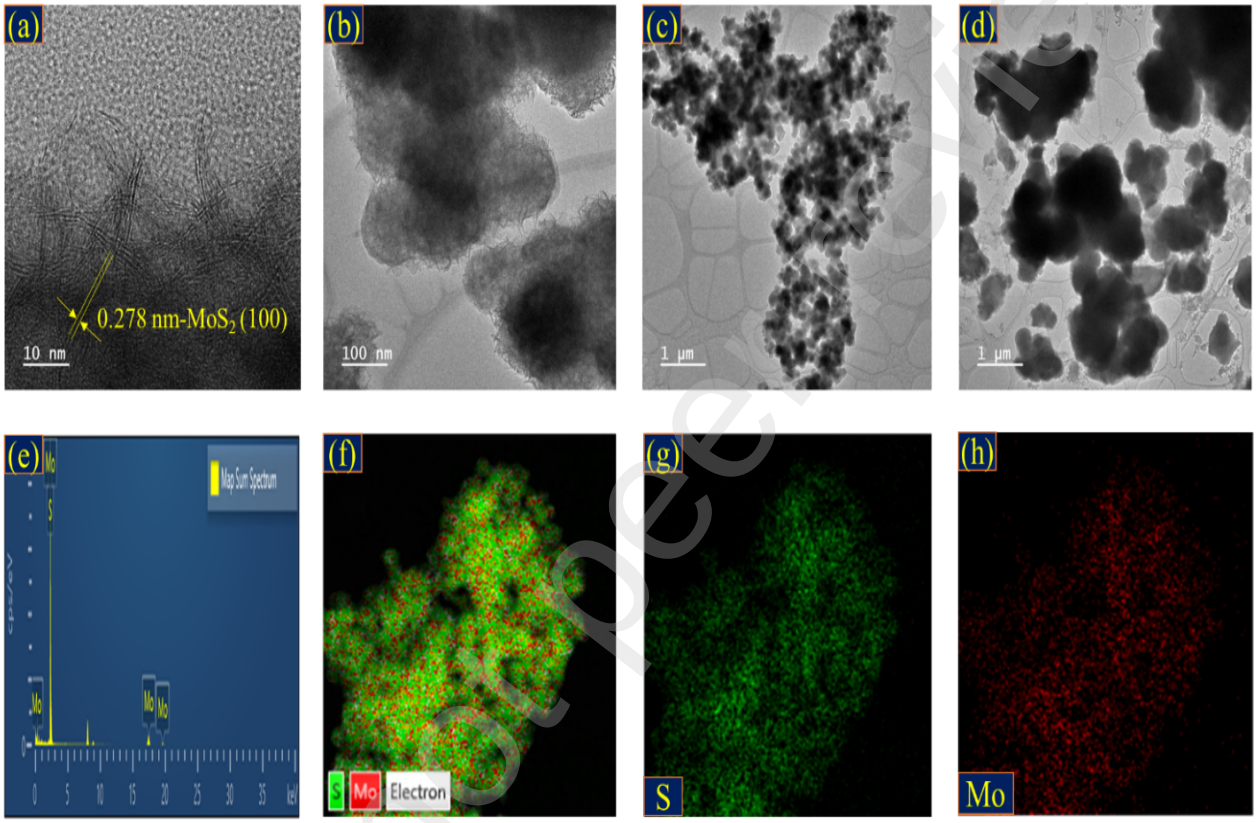

Figure 6. TEM images of (a)-(c) MoS_2 SNFs at various magnifications and (d) MoS_2 NFs. (e) EDX pattern of MoS_2 SNFs, (f)-(h) distributions of different elements on the MoS_2 SNFs surface.

3.3 Electrocatalytic activity for HER

Figure 7 describes the HER catalytic performances of the synthesized MoS_2 SNFs and NFs. The polarization curves of both catalysts and a Pt electrode in the 0.5 M H_2SO_4 standard electrolyte are shown in **Figure 7(a)**. The onset potentials of MoS_2 SNFs and NFs are equal to approximately −162 mV, indicating that the onset potential of MoS_2 depends not on its

morphology but on catalytic properties. However, the overpotentials of the prepared materials were significantly different at a current density of −50 mA·cm^{-2} (270 mV for MoS_2 SNFs and 345 mV for MoS_2 NFs). These results suggest that MoS_2 SNFs exhibit a significantly lower overpotential at the specified current density as compared with that of MoS_2 NFs, indicating much higher electrocatalytic activity of MoS_2 SNFs. The larger number of active sites and electrical conductivity of MoS_2 SNFs are important factors that contributed to their superior HER performance.

Another critical parameter used for evaluating the catalytic properties of an HER catalyst is a Tafel slope determined by Tafel analysis. The Tafel slope of a sample characterizes the reaction mechanism and catalytic activity. **Figure 7(b)** shows the Tafel slopes of the Pt electrode, MoS_2 SNFs, and MoS_2 NFs, which are equal to 34, 49, and 86 mV·dec^{-1}, respectively. The lower Tafel slope indicates the faster kinetics of the HER process; hence, MoS_2 SNFs exhibit better catalytic properties than those of MoS_2 NFs.

The impedances of the MoS_2 SNFs and NFs catalysts are displayed in **Figure 7(c)**. Here, the charge-transfer resistance includes the wire resistance (R_s), catalyst–electrolyte resistance (R_1), and catalyst–electrode resistance (R_2). Their values calculated for both catalysts are listed in **Table 2**. It is noteworthy that the charge-transfer resistance of MoS_2 SNFs (5.79 Ω) was significantly lower than that of MoS_2 NFs (26.08 Ω), indicating that the MoS_2 SNF surface was more conductive than that of MoS_2 NFs. This phenomenon can be explained by the smaller size of MoS_2 SNFs that increases both the density and conductivity of the catalyst. A low charge transfer resistance is highly beneficial for electrochemical applications. Moreover, the C_{dl} value of the synthesized MoS_2 SNFs (6.65 mF·cm^{-2}) was calculated from the results of CV studies conducted at different scan rates (see **Figures S2 and S3** in Supporting Information).

Table 2: Charge-transfer resistance list of MoS_2 SNFs and NFs

Material	R_s (Ω)	R_1 (Ω)	R_2 (Ω)
MoS_2 SNFs	8.55	5.79	3.59
MoS_2 NFs	9.81	26.08	16.2

During HER, hydrogen gas is released on the surface of cathode when protons (H^+) in solution receive electrons from the electrode under an applied voltage. The HER mechanism in acidic media could be described as follows:

$$H^+ + e^- = H_{ad} \quad \text{Volmer step}$$

$$H^+ + e^- + H_{ad} = H_2 \quad \text{Heyrovsky step}$$

$$H_{ad} + H_{ad} = H_2 \quad \text{Tafel step}$$

Because hydrogen gas is released from the cathode, the efficiency of hydrogen evolution strongly depends on the number of active sites on the electrode surface. Hence, catalysts with large active surface areas are beneficial for HER due to the faster electron transfer process. To determine the active surface areas of the prepared materials, the BET measurements were conducted for MoS_2 SNFs and NFs (the obtained results are presented in **Figure 7(d)**). The surface area of MoS_2 SNFs (98.2 $m^2 \cdot g^{-1}$) is significantly higher than that of MoS_2 NFs (7.01 $m^2 \cdot g^{-1}$), which is consistent with the results of a previous study [42]. The larger surface area of

MoS_2 SNFs is the main reason for its better HER performance as compared with that of MoS_2 NFs.

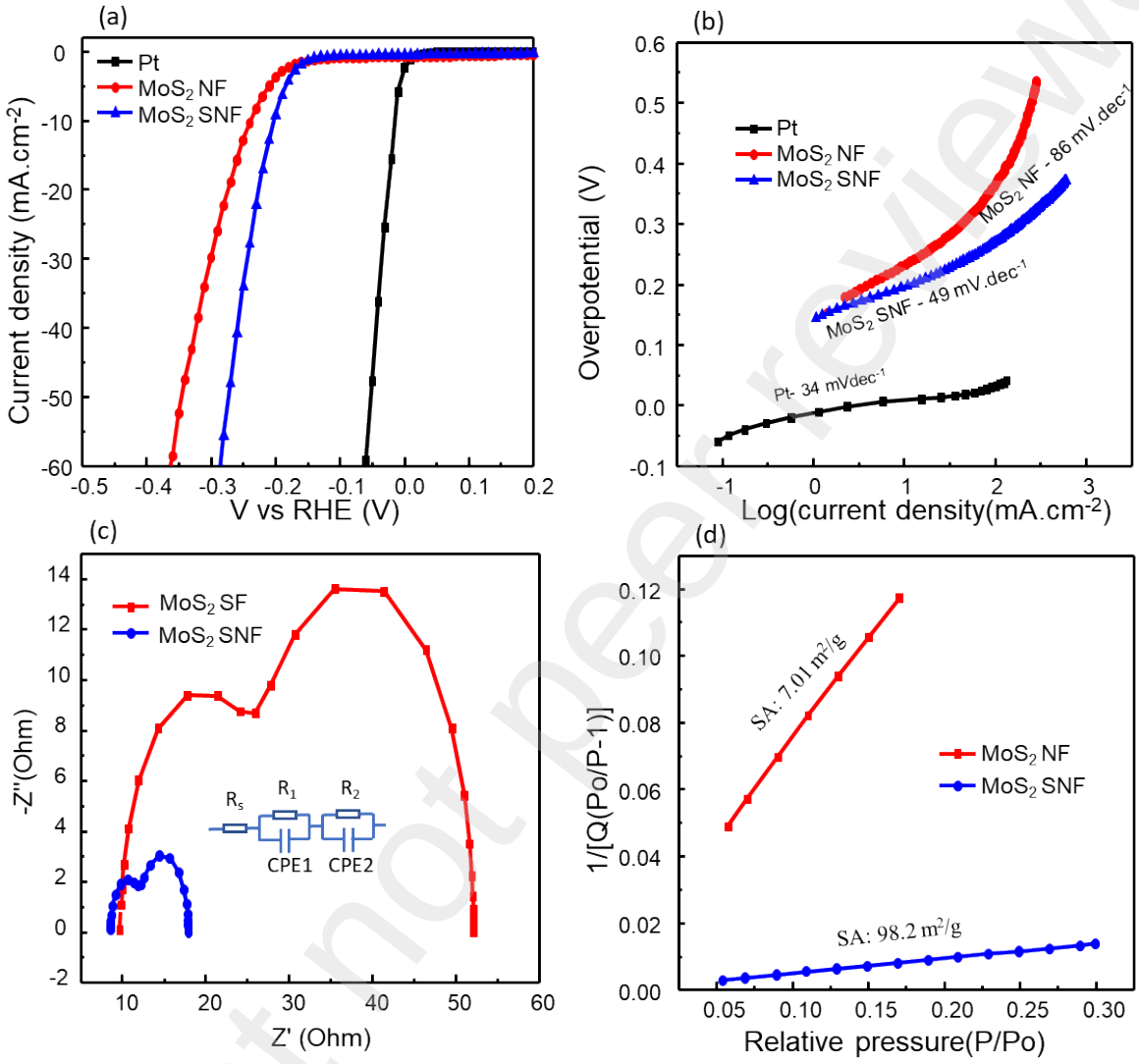

Figure 7. (a) Polarization curves, (b) Tafel slopes, (c) EIS curves, and (d) BET surface areas of the prepared MoS_2 SNFs and NFs.

The stability of the synthesized MoS_2 SNFs toward HER was evaluated by conducting CA and CV tests in acidic media. The CA test was continuously performed for 12 h, after which the sample was subjected to 1000 CV cycles. The obtained CV and CA data are presented in **Figures S4** and **S5**, respectively. Subsequently, the sample was examined by LSV, and its Tafel

slope was recalculated. **Figures 8(a)** and **(b)** display the LSV curves and Tafel slopes of MoS_2 SNFs obtained before and after the stability tests. They show that the change in the LSV curve after testing was negligible while the Tafel slope slightly increased from 49 to 51 $mV \cdot cm^{-2}$, indicating the superior stability of MoS_2 SNFs in acidic media.

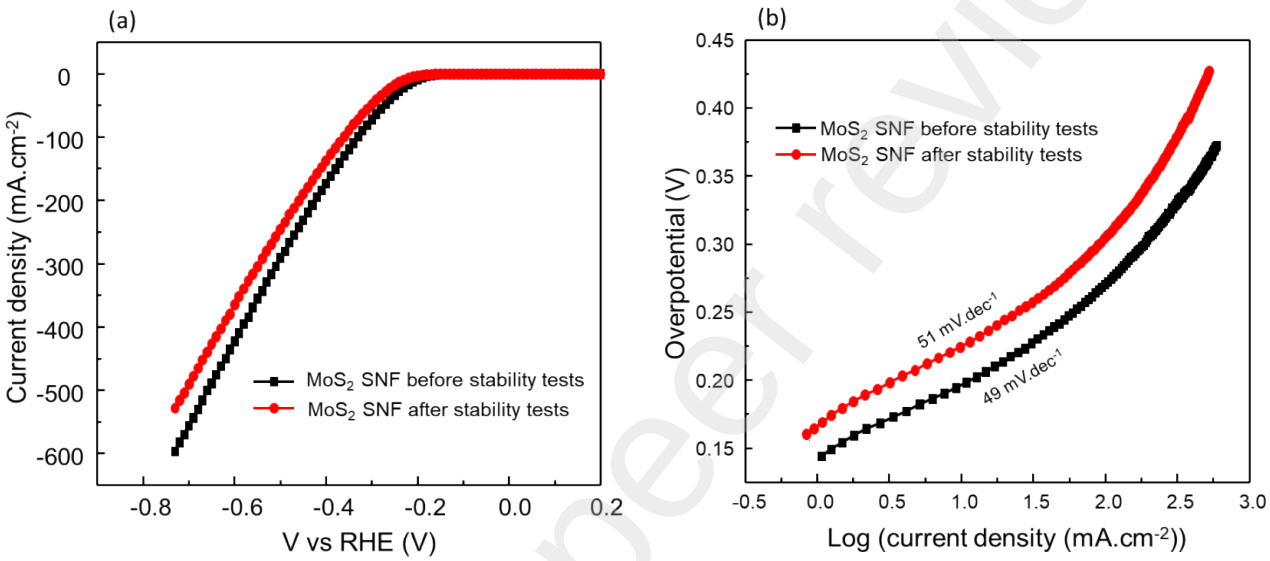

Figure 8. HER performances of MoS_2 SNFs observed before and after the CA and CV stability tests: (a) polarization curves and (b) Tafel slopes.

4. Conclusion

In this study, MoS_2 SNFs were successfully prepared, and their morphology and HER catalytic properties were investigated. The size of MoS_2 SNFs (50–70 nm) was significantly smaller than that of MoS_2 NFs (600–950 nm), which was highly beneficial for electrochemical applications. The in situ doped nitrogen of the fabricated catalyst also enhanced its catalytic properties. The synthesized material exhibited high performance during HER with a low Tafel slope of 49 $mV \cdot dec^{-1}$, an overpotential of 270 mV at a current density of 50 $mA \cdot cm^{-2}$, a large

surface area of 98 $m^2 \cdot g^{-1}$, and unprecedented stability in the acidic environment. The obtained results indicate that MoS_2 SNFs is a promising catalytic material for energy storage and chemical applications.

Supporting Information

Supporting Information contains XPS survey spectra of MoS_2 SNFs; CV curves of MoS_2 SNFs recorded at different scan rates; calculated C_{dl} of MoS_2 SNFs; results of the CA stability test of MoS_2 SNFs conducted for 12 h; and results of the CV stability test of MoS_2 SNFs obtained after 1000 cycles.

The authors declare that they have no competing interests.

Acknowledgments

This research was supported by NRF funded by the Korean government [grant numbers 2021R1A4A3027878, 2022M3H4A1A01012712].

References

[1] J. Xi, X. Huang, M. Hu, W. Xiang, Dependence of laser parameters on structural properties of pulsed laser-deposited MoS_2 thin films applicable for field effect transistors, Journal of Materials Science: Materials in Electronics. 31 (2020) 21118-21127.

[2] M. Yue, H. Lambert, E. Pahon, R. Roche, S. Jemei, D. Hissel, Hydrogen energy systems: A critical review of technologies, applications, trends and challenges, Renewable and Sustainable Energy Reviews. 146 (2021) 111180.

[3] W. Lubitz, W. Tumas, Hydrogen: an overview, Chemical reviews. 107 (2007) 3900-3903.

[4] D.W. Boukhvalov, A. Marchionni, J. Filippi, C.-N. Kuo, J. Fujii, R. Edla, S. Nappini, G. D'Olimpio, L. Ottaviano, C.S. Lue, Efficient hydrogen evolution reaction with platinum stannide $PtSn_4$ via surface oxidation, Journal of Materials Chemistry A. 8 (2020) 2349-2355.

[5] Y. Wu, J. Yao, J. Gao, Interface chemistry of platinum-based materials for electrocatalytic hydrogen evolution in alkaline conditions, Methods for Electrocatalysis, Springer, 2020, 453-473.

[6] D. Wu, K. Kusada, T. Yamamoto, T. Toriyama, S. Matsumura, I. Gueye, O. Seo, J. Kim, S. Hiroi, O. Sakata, On the electronic structure and hydrogen evolution reaction activity of platinum group metal-based high-entropy-alloy nanoparticles, Chemical science. 11 (2020) 12731-12736.

[7] J. Zheng, W. Sheng, Z. Zhuang, B. Xu, Y. Yan, Universal dependence of hydrogen oxidation and evolution reaction activity of platinum-group metals on pH and hydrogen binding energy, Science advances. 2 (2016) 1501602.

[8] C. Wang, H. Shang, H. Xu, Y. Du, Nanoboxes endow non-noble-metal-based electrocatalysts with high efficiency for overall water splitting, Journal of Materials Chemistry A. 9 (2021) 857-874.

[9] H. Wu, C. Feng, L. Zhang, J. Zhang, D.P. Wilkinson, Non-noble metal electrocatalysts for the hydrogen evolution reaction in water electrolysis, Electrochemical Energy Reviews. 4 (2021) 473-507.

[10] J. Wang, F. Xu, H. Jin, Y. Chen, Y. Wang, Non-noble metal-based carbon composites in hydrogen evolution reaction: fundamentals to applications, Advanced materials. 29 (2017) 1605838.

[11] J. Wang, J. Liu, B. Zhang, X. Ji, K. Xu, C. Chen, L. Miao, J. Jiang, The mechanism of hydrogen adsorption on transition metal dichalcogenides as hydrogen evolution reaction catalyst, Physical Chemistry Chemical Physics. 19 (2017) 10125-10132.

[12] S. Mansingh, K.K. Das, K. Parida, HERs in an acidic medium over MoS_2 nanosheets: from fundamentals to synthesis and the recent progress, Sustainable Energy & Fuels. 5 (2021) 1952-1987.

[13] Y. Huang, Y. Sun, X. Zheng, T. Aoki, B. Pattengale, J. Huang, X. He, W. Bian, S. Younan, N. Williams, Atomically engineering activation sites onto metallic 1T-MoS_2 catalysts for enhanced electrochemical hydrogen evolution, Nature communications. 10 (2019) 1-11.

[14] J.H. Lee, Y.S. Park, M.J. Jang, S.M. Park, K.H. Lee, W.S. Choi, S.M. Choi, Y.D. Kim, MoS_2/CNFs derived from electrospinning and heat treatment as the efficient electrocatalyst for hydrogen eovlution reaction in acidic solution, Korean Journal of Metals and Materials. 56 (2018) 885-892.

[15] C. Liu, C. Kong, F. J. Zhang, C. M. Kai, W. Q. Cai, X. Y. Sun, W. C. Oh, Research progress of defective MoS_2 for photocatalytic hydrogen evolution, Journal of the Korean Ceramic Society. 58 (2021) 135-147.

[16] H. Wang, C. Li, P. Fang, Z. Zhang, J. Z. Zhang, Synthesis, properties, and optoelectronic applications of two-dimensional MoS_2 and MoS_2-based heterostructures, Chemical Society Reviews. 47 (2018) 6101-6127.

[17] Z. Zheng, L. Yu, M. Gao, X. Chen, W. Zhou, C. Ma, L. Wu, J. Zhu, X. Meng, J. Hu, Boosting hydrogen evolution on MoS_2 via co-confining selenium in surface and cobalt in inner layer, Nature communications. 11 (2020) 1-10.

[18] F. J. Zhang, C. Kong, X. Li, X. Y. Sun, W. J. Xie, W. C. Oh, F. J. Zhang, C. Kong, X. Li, X.-Y. Sun, Synthesis and characterization of MoS_2/Graphene-TiO_2 ternary photocatalysts for high-efficiency hydrogen production under visible light, Journal of the Korean Ceramic Society. 56 (2019) 284-290.

[19] L. Luo, M. Shi, S. Zhao, W. Tan, X. Lin, H. Wang, F. Jiang, Hydrothermal synthesis of MoS_2 with controllable morphologies and its adsorption properties for bisphenol A, Journal of Saudi Chemical Society. 23 (2019) 762-773.

[20] D. Gupta, V. Chauhan, R. Kumar, A comprehensive review on synthesis and applications of molybdenum disulfide (MoS_2) material: Past and recent developments, Inorganic Chemistry Communications. 121 (2020) 108200.

[21] U. Krishnan, M. Kaur, K. Singh, M. Kumar, A. Kumar, A synoptic review of MoS_2: Synthesis to applications, Superlattices and Microstructures. 128 (2019) 274-297.

[22] D. Wang, Z. Pan, Z. Wu, Z. Wang, Z. Liu, Hydrothermal synthesis of MoS_2 nanoflowers as highly efficient hydrogen evolution reaction catalysts, Journal of Power Sources. 264 (2014) 229-234.

[23] C. B. Ma, X. Qi, B. Chen, S. Bao, Z. Yin, X. J. Wu, Z. Luo, J. Wei, H. L. Zhang, H. Zhang, MoS_2 nanoflower-decorated reduced graphene oxide paper for high-performance hydrogen evolution reaction, Nanoscale. 6 (2014) 5624-5629.

[24] Y. Lu, X. Yao, J. Yin, G. Peng, P. Cui, X. Xu, MoS_2 nanoflowers consisting of nanosheets with a controllable interlayer distance as high-performance lithium ion battery anodes, RSC Advances. 5 (2015) 7938-7943.

[25] S. Mishra, P.K. Maurya, A.K. Mishra, 2H–MoS_2 nanoflowers based high energy density solid state supercapacitor, Materials Chemistry and Physics. 255 (2020) 123551.

[26] S.S. Singha, S. Rudra, S. Mondal, M. Pradhan, A. K. Nayak, B. Satpati, P. Pal, K. Das, A. Singha, Mn incorporated MoS_2 nanoflowers: A high performance electrode material for symmetric supercapacitor, Electrochimica Acta. 338 (2020) 135815.

[27] G. Ghanashyam, H.K. Jeong, Size Effects of MoS_2 on hydrogen and oxygen evolution reaction, Journal of Electrochemical Science and Technology. 13 (2021) 120-127.

[28] S. Bolar, S. Shit, J.S. Kumar, N.C. Murmu, R.S. Ganesh, H. Inokawa, T. Kuila, Optimization of active surface area of flower like MoS_2 using V-doping towards enhanced hydrogen evolution reaction in acidic and basic medium, Applied Catalysis B: Environmental. 254 (2019) 432-442.

[29] C. Tsai, F. Abild-Pedersen, J.K. Nørskov, Tuning the MoS_2 edge-site activity for hydrogen evolution via support interactions, Nano letters. 14 (2014) 1381-1387.

[30] X. Huang, Z. Zeng, S. Bao, M. Wang, X. Qi, Z. Fan, H. Zhang, Solution-phase epitaxial growth of noble metal nanostructures on dispersible single-layer molybdenum disulfide nanosheets, Nature communications. 4 (2013) 1-8.

[31] Y. Wang, S. LIu, X. Hao, S. Luan, H. You, J. Zhou, D. Song, D. Wang, H. Li, F. Gao, Surface reorganization engineering of the N-doped MoS_2 heterostructures MoO x@ N-doped MoS_{2-x} by in situ electrochemical oxidation activation for efficient oxygen evolution reaction, Journal of Materials Chemistry A. 7 (2019) 10572-10580.

[32] H. Dong, C. Liu, H. Ye, L. Hu, B. Fugetsu, W. Dai, Y. Cao, X. Qi, H. Lu, X. Zhang, Three-dimensional nitrogen-doped graphene supported molybdenum disulfide nanoparticles as an advanced catalyst for hydrogen evolution reaction, Scientific reports. 5 (2015) 1-11.

[33] S. Hu, W. Chen, J. Zhou, F. Yin, E. Uchaker, Q. Zhang, G. Cao, Preparation of carbon coated MoS_2 flower-like nanostructure with self-assembled nanosheets as high-performance lithium-ion battery anodes, Journal of Materials Chemistry A. 2 (2014) 7862-7872.

[34] H. Zhang, H. Lin, Y. Zheng, Y. Hu, A. MacLennan, Understanding of the effect of synthesis temperature on the crystallization and activity of nano-MoS_2 catalyst, Applied Catalysis B: Environmental. 165 (2015) 537-546.

[35] A. Bahuguna, S. Kumar, V. Sharma, K.L. Reddy, K. Bhattacharyya, P. Ravikumar, V. Krishnan, Nanocomposite of MoS_2-RGO as facile, heterogeneous, recyclable, and highly efficient green catalyst for one-pot synthesis of indole alkaloids, ACS Sustainable Chemistry & Engineering. 5 (2017) 8551-8567.

[36] Z. Guo, J. Dong, H. Zhu, Y. Gong, P. Li, D. Yang, X. Shan, Y. Wang, L. Zheng, Y. Zhao, Comparative investigation of the vibrational properties of bulk 2H–MoS_2 and its exfoliated nanosheets under high pressure, Journal of Raman Spectroscopy. 48 (2017) 596-600.

[37] P. Qin, G. Fang, W. Ke, F. Cheng, Q. Zheng, J. Wan, H. Lei, X. Zhao, In situ growth of double-layer MoO_3/MoS_2 film from MoS_2 for hole-transport layers in organic solar cell, Journal of Materials Chemistry A. 2 (2014) 2742-2756.

[38] M. Li, Y. C. Kuo, X. Chu, D. Chu, J. Yi, MoS_2 nanoflower incorporated with Au/Pt nanoparticles for highly efficient hydrogen evolution reaction, Emergent Materials. 4 (2021) 579-587.

[39] S. Wang, D. Zhang, B. Li, C. Zhang, Z. Du, H. Yin, X. Bi, S. Yang, Ultrastable in-plane 1T–2H MoS_2 heterostructures for enhanced hydrogen evolution reaction, Advanced Energy Materials. 8 (2018) 1801345.

[40] C. Backes, R. J. Smith, N. McEvoy, N. C. Berner, D. McCloskey, H. C. Nerl, A. O'Neill, P.J. King, T. Higgins, D. Hanlon, Edge and confinement effects allow in situ measurement of size and thickness of liquid-exfoliated nanosheets, Nature communications. 5 (2014) 1-10.

[41] Q. Zhao, Q. Ma, F. Pan, Z. Wang, B. Yang, J. Zhang, J. Zhang, Facile synthesis of nitrogen-doped carbon nanosheets as metal-free catalyst with excellent oxygen reduction performance in alkaline and acidic media, Journal of Solid State Electrochemistry. 20 (2016) 1469-1479.

[42] T. Van Nguyen, M. Tekalgne, T.P. Nguyen, W. Wang, S.H. Hong, J.H. Cho, Q. Van Le, H.W. Jang, S. H. Ahn, S. Y. Kim, Control of the morphologies of molybdenum disulfide for hydrogen evolution reaction, International Journal of Energy Research. 46 (2022) 11479-11491.